This is the accepted manuscript made available via CHORUS. The article has been published as:

Local density of states induced near impurities in Mott insulators

Wenxin Ding and Qimiao Si

Phys. Rev. B **110**, L081104 — Published 5 August 2024

DOI: 10.1103/PhysRevB.110.L081104

Local Density of States induced near Impurities in Mott Insulators

Wenxin Ding[1,2,3*] and Qimiao Si[2]
[1]*School of Physics and Optoelectronics Engineering, Anhui University, Hefei, Anhui Province, 230601, China*
[2]*Department of Physics & Astronomy, Rice University, Houston, Texas 77005, USA*
[3]*Kavli Institute for Theoretical Sciences, University of Chinese Academy of Sciences, Beijing, 100049, China*
(Dated: July 2, 2024)

The local density of states near dopants or impurities has recently been probed by scanning tunneling microscopy in both the parent and very lightly doped compounds of the high-T_c cuprate superconductors. We use a slave-rotor representation of the Hubbard model to compute the local density of states on impurities in a Mott insulator. Our calculation accounts for the following key features of the experimental observation: i) positions and amplitudes of the in-gap spectral weights of a single impurity; ii) the spectral weight transfer from the upper Hubbard band to the lower Hubbard band; iii) the difference between the cases of single and multiple impurities. For multiple impurities, our study explains the complete suppression of spectral weight observed at precisely the Fermi energy and links this property to zeros of the underlying bulk Green's function of the Mott insulating phase.

Introduction. The high-T_c cuprate superconductors are generally interpreted as doped Mott insulators[1]. The undoped parent compounds are ordered antiferromagnetically. Although the parent compounds are three-band, charge transfer insulators[2], it is believed that the single-band Hubbard model (HM) provides an adequate effective description. The strong, onsite Coulomb repulsion, Hubbard-U, forbids two electrons to occupy the same Cu site, thereby creating a Mott gap $\propto U$. As a result, the electronic spectrum splits into an upper Hubbard band (UHB) and a lower Hubbard band (LHB). Superconductivity arises from carrier-doping the parent compounds beyond a threshold concentration.

The rich properties of the doped cuprates suggest the importance of studying Mott insulators with dilute dopants or impurities. The local density of states (LDOS) near dopants or impurities in the parent Mott insulator has been studied through scanning tunneling microscope (STM) measurements[4, 5]. These experiments have uncovered a number of features on the electronic excitation spectrum of a Mott insulator. For a single impurity, the in-gap states emerge from the UHB above the Fermi energy. When impurity concentration increases, the in-gap states gradually fill up the Mott gap, but a "V"-shaped dip forms near the Fermi energy. The observed dip means that the impurities or dopants cannot produce in-gap states exactly at the Fermi energy.

The experimental development is exciting as it bridges between the clean parent compounds and the heavily debated, lightly doped but metallic pseudogap regimes[6]. A systematic study of the Mott insulator in the presence of a single defect dopant or impurity is highly desirable. Previous efforts on this type of problems[7–9] have been mostly numerical, which are restricted by finite-size effect, and have yet to achieve the understanding of the key experimental observations mentioned earlier.

In this Letter, we study the LDOS of single and multiple impurities in a Mott insulator based on a slave rotor representation of the HM in the thermodynamic limit. We find clear, impurity-induced in-gap bound states, descending from the UHB as observed in Ref. [4] in $Ca_2CuO_2Cl_2$(CCOC). In addition, we obtain the correct spectral weight transfer from the UHB to the LHB. Systematic calculations of the bound state energies and their corresponding spectral weights provide qualitative understanding about the experiments of Ref. [5] which is done for $Bi_2Sr_{2-x}La_xCuO_{6+\delta}$(La-Bi2201) at two hole densities $p = 0.03$ and 0.07: i) the bound states cannot reach the Fermi energy; ii) the bound states with energies closer to the Fermi energy have smaller spectral weights. We further show that the vanishing of the LDOS at the Fermi energy reflects the zeros of the Green's function, i.e the Luttinger surface[10], of the underlying Mott insulator. That is a feature of considerable interest to the Mott insulator per se and to the physics of the pseudogap regime of the underdoped cuprates [11–13]. Recently, similar LDOS on apical oxygen impurities are also observed in a different Mott insulator Sr_2IrO_4[14].

The slave-rotor approach. We consider the single band Hubbard model on a square lattice

$$H_{HM} = \sum_i H_{at}(i) - \sum_{ij,\sigma}(t_{ij} d^\dagger_{i\sigma} d_{j\sigma} + H.c.), \qquad (1)$$

in which $H_{at}(i) = \frac{U}{2}(n_\uparrow - 1/2)(n_\downarrow - 1/2)$. For simplicity, we consider only hopping between nearest-neighbor (nn) sites, $\langle ij \rangle$. The full energy spectrum of $H_{at}(i)$ can be economically represented by a rotor kinetic energy $H_{at}(i) \to U\hat{L}_i^2/2$ [16, 17] with $\hat{L}_i = -i\partial_{\theta_i}$, which provides a tractable reference point for perturbative expansion in t/U. In this slave-rotor representation, the bare electron operator is written as a product of the rotor field and a fermionic spinon operator $d_{i\alpha} \equiv f_{i\alpha} e^{-i\theta_i}$, with the constraint

$$\hat{L}_i = \sum_\sigma (f^\dagger_{i\sigma} f_{i\sigma} - 1/2). \qquad (2)$$

In place of the phase field one could work with the complex field $e^{i\theta_i} = X_i$, with the additional constraint $|X_i|^2 = 1$. The two constraints are enforced by introducing two Lagrangian multipliers, h_i and λ_i. In terms of the fermionic f_i and complex rotor X_i operators, the physical d_i-electron operator at site i is expressed as follows:

$$d_{i\sigma} \equiv f_{i\sigma} X_i^* \,. \tag{3}$$

Correspondingly, the rotor operator becomes $\hat{L}_i = (h - X_i^* \partial_t X_i)/U$.

Intuitively, in the Mott phase, the rotor fields describe the bosonic Hubbard-U charge dynamics while the f-spinons describe the magnetic fluctuations. It is shown in Ref. [15] that by integrating out the X-fields, the Heisenberg interaction term is correctly recovered with the physical spins given by the f-spinons as $\boldsymbol{S}_i = \sum_{\alpha,\beta} f_\alpha^\dagger \boldsymbol{\sigma}_{\alpha\beta} f_\beta$.

A saddle point solution[17, 18] (see Supplemental Materials, Eq. (S-1) for details) is found for a paramagnetic Mott insulating phase. This saddle point state is described by a free f-spinon theory and a free X-field theory. Their corresponding Green's functions are

$$G_{f,0}(\omega; \boldsymbol{k}) = (\omega + h - Q_f \epsilon_{\boldsymbol{k}})^{-1}, \tag{4}$$

$$G_{X,0}(\nu; \boldsymbol{k}) = (-\nu^2/U + 2ih\nu/U + \lambda + Q_X \epsilon_{\boldsymbol{k}})^{-1}, \tag{5}$$

where $\epsilon_{\boldsymbol{k}} = -2t(\cos k_x + \cos k_y)$ is the bare lattice dispersion function, $Q_f = Q_{f\langle ij\rangle} = \langle X_j^* X_i\rangle$, $Q_{X\langle ij\rangle} = \langle \sum_\sigma f_{j\sigma}^\dagger f_{i\sigma}\rangle$. The spin and charge sectors are coupled through the self-consistency between Q_f and Q_X. Although we only consider the nn hopping in this work, the inclusion of other hopping terms such as the next-nearest-neighbor term would only renormalize Q_f and Q_x. According to Eq. (3), the electronic Green's function is calculated via the rotor and spinon Green's functions according to

$$iG_d(t; \boldsymbol{x}, \boldsymbol{x}') = -G_f(t; \boldsymbol{x}, \boldsymbol{x}') G_X(-t; \boldsymbol{x}, \boldsymbol{x}'). \tag{6}$$

We focus on the electronic LDOS $\rho_d(\omega; \boldsymbol{x}) = -(\pi)^{-1}\Im m[G_d^R(\omega; \boldsymbol{x}, \boldsymbol{x})]$, expressed as

$$\begin{aligned}\rho_d(\omega; \boldsymbol{x}) = &\int d\omega' \rho_f(\omega'; \boldsymbol{x}) \rho_X(\omega - \omega'; \boldsymbol{x}) \\ &\times (n_f(\omega') + n_B(\omega - \omega')),\end{aligned} \tag{7}$$

where $\rho_f[\omega; \boldsymbol{x}] = -(\pi)^{-1}\Im m[G_f^R(\omega)]$, and $\rho_X[\omega] = -(\pi)^{-1}\Im m[G_X^R(\omega)]$.

In this work, we are interested in the large-U limit in which $\lambda \simeq U/4$ [15]. At the saddle point, $\Im m[G_f(\omega')]$ centers at $\omega' = 0$ with a bandwidth $W_f = 4D\, t\, Q_f$, which is small because $t\, Q_f \ll U$; any impurity effects on $\Im m[G_f(\omega')]$ *per se* would be on the same scale. In the convolution, $\Im m[G_f(\omega')]$ can be regarded as a broadened δ-function since $Q_f \ll U$. The Mott gap is primarily determined by $\Im m[G_X(\nu)]$. Therefore, the impurity-induced features of the electronic LDOS are mainly determined by the rotor fields, which shall be our focus in the following.

The induced rotor impurity potential.

We consider the case of a single impurity in CCOC as experimentally studied in Ref. [4], which is either a missing chlorine(Cl^-) ion or a calcium(Ca^{2+}) defect. The vacancy is charged and creates an impurity potential. We model it by a localized, onsite potential $V(\boldsymbol{x}_i)$, where $\boldsymbol{x}_i$ denotes the vacancy position.

Consider a single on-site impurity at $\boldsymbol{x}_0$:

$$H_1 = V \sum_\sigma d_{\boldsymbol{x}_0,\sigma}^\dagger d_{\boldsymbol{x}_0,\sigma} = V \sum_\sigma f_{\boldsymbol{x}_0,\sigma}^\dagger f_{\boldsymbol{x}_0,\sigma}. \tag{8}$$

This bare impurity potential only couples to the spinons and induces a variation of the local spinon density $\delta n_f(\boldsymbol{x}_0) = \delta\langle\sum_\sigma f_{\boldsymbol{x}_0\sigma}^\dagger f_{\boldsymbol{x}_0\sigma}\rangle$. However, the rotors and the spinons are subject to the constraint Eq. (2). Through the constraint, the rotors will be perturbed by the impurity potential as well.

In the large-U case, it suffices to solve the constraint in the atomic limit. For the bulk state, we have $\langle\hat{L}\rangle = 0 \to h = 0$. For arbitrary h, we have

$$\langle\hat{L}\rangle = h/U - \frac{1}{2}\frac{h}{\sqrt{-h^2 + \lambda U}}. \tag{9}$$

Therefore, $\delta n_f(\boldsymbol{x}_0)$ further induces a variation of the Lagrangian multiplier h through the constraint which we shall label as $\delta h(\boldsymbol{x}_0)$. Using the atomic limit result, $\delta h(\boldsymbol{x}_0)$ is obtained by solving the following equation:

$$\frac{\delta h(\boldsymbol{x}_0)}{U} - \frac{\delta h(\boldsymbol{x}_0)}{2\sqrt{-\delta h(\boldsymbol{x}_0)^2 + \lambda U}} = \delta\langle n_f(\boldsymbol{x}_0)\rangle. \tag{10}$$

Taking $\lambda = U/4$, we plot the solution of $\delta h(\boldsymbol{x}_0)$ as a function of $\delta\langle n_f(\boldsymbol{x}_0)\rangle$ in Fig. (1a). To solve for the impurity states, we take $\delta\langle n_f(\boldsymbol{x}_0)\rangle = -1$, since V of relevance to the experiments is on the order of eV, i.e. much larger than the spinons' bandwidth. This solution gives us the upper bound of $h(\boldsymbol{x}_0)$. For the rest of this work, we shall use $\delta h(\boldsymbol{x}_0) \simeq 0.473U$ unless specified otherwise. Even though negative solutions of $\delta h(\boldsymbol{x}_0)$ are allowed here, they do not induce in-gap bound states, and thus shall be ignored. Then the rotor impurity potential due to $\delta h(\boldsymbol{x}_0)$ is

$$\hat{H}_{X,\boldsymbol{x}_0} = ih_0(X_{\boldsymbol{x}_0}^* \partial_t X_{\boldsymbol{x}_0} - X_{\boldsymbol{x}_0} \partial_t X_{\boldsymbol{x}_0}^*) \tag{11}$$

where we label $h_0 = 2\delta h(\boldsymbol{x}_0)/U$.

Impurity state Green's function. We now turn to calculate the LDOS of a single impurity in a Mott insulator using the T-matrix formalism. The full rotor Green's function, to the first order in h_0 can be expressed as

$$\begin{aligned}G_X(\nu; \boldsymbol{x}_1, \boldsymbol{x}_2) &= G_{X,0}(\nu; \boldsymbol{x}_1, \boldsymbol{x}_2) \\ &+ G_{X,0}(\nu; \boldsymbol{x}_1, \boldsymbol{x}_0)\langle\boldsymbol{x}_0|\hat{T}|\boldsymbol{x}_0\rangle G_{X,0}(\nu; \boldsymbol{x}_0, \boldsymbol{x}_2).\end{aligned} \tag{12}$$

Here, the rotor T-matrix is defined as

$$\hat{T} = \frac{\hat{H}_{X,\boldsymbol{x}_0}}{1 - h_0 \nu G_{X,0}(\nu; \boldsymbol{x}_0, \boldsymbol{x}_0)}, \tag{13}$$

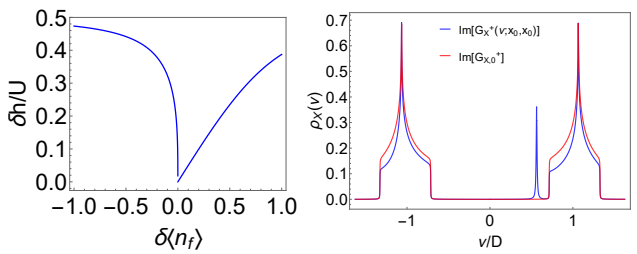


FIG. 1. (Color online) (1a) the solution of $\delta h(x_0)$ plotted as a function of $\delta\langle n_f(x_0)\rangle$; (1b) the bulk rotor spectral function $\Im m[G^+_{X,0}(\omega;\boldsymbol{x},\boldsymbol{x})]$ (blue) compared with that on a single impurity, $\Im m[G^+_X(\omega;\boldsymbol{x}_0,\boldsymbol{x}_0)]$ (red) .

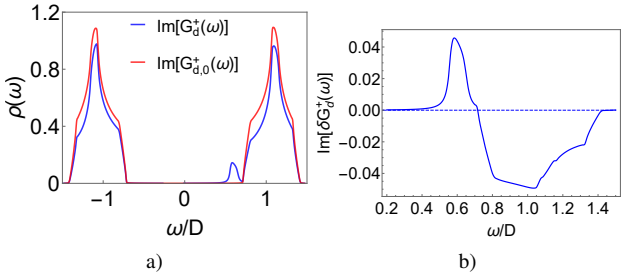


FIG. 2. (Color online) electronic LDOS on the impurity site (blue) compared with the bulk (red) (2a), and the variation of LDOS on the impurity(2b).

where $|\boldsymbol{x}\rangle$ is the bulk rotor eigenfunction in the spatial representation.From here on, we abbreviate notations by writing $G_{X,0}(\nu;\boldsymbol{x}_i,\boldsymbol{x}_j) = g_{ij}$. Similarly, the retarded bulk rotor Green's function is written as $G^+_{X,0}(\nu;\boldsymbol{x}_i,\boldsymbol{x}_j) = g^+_{ij}$. The impurity induced variation of the local rotor spectral function $\delta\rho_X(\nu;\boldsymbol{x}) = \rho_X(\nu;\boldsymbol{x}) - \rho_{X,0}(\nu;\boldsymbol{x})$ is derived from the retarded $\hat{T}$ matrix:

$$\delta\rho_X(\nu;\boldsymbol{x}_l) = -\frac{1}{\pi}\Im m[\frac{h_0\nu g^+_{0l}g^+_{l0}}{1-h_0\nu g^+_{00}}]. \tag{14}$$

It is convenient to separately discuss the two pieces of $\delta\rho_X(\nu;\boldsymbol{x})$: i) the first piece $\delta\rho_{X,1}(\nu;\boldsymbol{x}_0)$ comes from the original poles of g^+_{00}, i.e. the correction to the bulk Hubbard band, which reads

$$\delta\rho_{X,1}(\nu;\boldsymbol{x}_0) = \frac{2h_0\nu\rho_0(\nu)\Lambda_0(\nu)(1-h_0\nu\Lambda_0(\nu))}{(1-h_0\nu\Lambda_0(\nu))^2+\pi^2\rho_0(\nu)^2}, \tag{15}$$

where $\Lambda_0(\nu) = \Re e[g^+_{00}]$ and $\rho_0(\nu) = -\Im m[g^+_{00}]/\pi$; ii) the second contribution $\delta\rho_{X,2}(\nu;\boldsymbol{x}_0)$ comes from new poles that correspond to the vanishing denominator $1-h_0\nu g_{00}$. The new poles are only possible where $\rho_0(\nu;\boldsymbol{x}) \to 0$, i.e., for our concern, inside the Mott gap. $\delta\rho_{X,2}(\nu;\boldsymbol{x}_0)$ is expressed as

$$\delta\rho_{X,2}(\nu;\boldsymbol{x}_0) = \frac{h_0\nu(\Lambda_0(\nu)^2-\pi^2\rho_0(\nu)^2)}{|h_0(\nu\,\partial_\nu\Lambda_0(\nu)+\Lambda_0(\nu))|}\delta(\nu-\nu_b). \tag{16}$$

The energy of the bound state ν_b is found by numerically solving the equation (see Fig. (S1) for numerical results of g_{00})

$$1-h_0\nu g_{00} = 0. \tag{17}$$

Through Eq. (7), we see that ν_b determines the center of the electronic in-gap spectral weights.

We show in Fig. (1b) the bulk rotor spectral function (red) and that on the impurity (blue). The Dirac-δ function is broadened as a Lorentzian.

The electronic spectral function obtained through Eq. (14) is shown in Fig. (2a) and variation of the spectral function $\delta\rho_d(\omega;\boldsymbol{x}_0) = \rho_d(\omega;\boldsymbol{x}_0) - \rho_{d,0}(\omega;\boldsymbol{x}_0)$ is given in Fig. (2b). Both are in good agreement with the experimental results of Ref.[4], which we quote in Supplemental Materials. Even though the experimental data are in arbitrary units, the relative area under the peak and above the dip in Fig. (2b) is still quantitatively comparable to the experimental results.

Solution for multiple impurities. The single impurity solution considered above is already the upper bound in terms of bound state energies, which are very close to the UHB. However, in the experiments for the Ca^{2+} vacancy of Ref. [4], the bound state is closer to the Fermi energy. In the finite doping but still insulating cases[5], the binding energies of the in-gap states are way beyond this limit. They can actually approach the Fermi energy but never reach it. The spectral weight of the in-gap states forms a sharply V-shaped feature centered at the Fermi energy. We now show that, by considering multiple impurities, these properties are also captured within our framework: i) bound states of similar energies superimpose to create new bound states with smaller energies; ii) such bound states carry smaller spectral weights compared to that of the single impurity case.

For simplicity, we start with the two-impurity case. We label their positions as $\boldsymbol{x}_1$ and $\boldsymbol{x}_2$, and their corresponding single-impurity T-matrices as $\hat{T}_1$ and $\hat{T}_2$ which are similarly defined in Eq. (13). To the lowest order, the full T-matrix is given by [19]

$$\hat{T} = f_{12}(\hat{T}_1+\hat{T}_2+\hat{T}_1g_{12}\hat{T}_2+\hat{T}_2g_{21}\hat{T}_1), \tag{18}$$

with $f_{12} = (1-t_1t_2g_{12}g_{21})^{-1}$, and $t_i = \nu h_0(\boldsymbol{x}_i)(1-\nu h_0(\boldsymbol{x}_i)g_{ii})^{-1}$. Both $\hat{T}_1$ and $\hat{T}_2$ contribute in-gap bound states at their own $\nu_{b,1(2)}$. Moreover, the factor f_{12} contributes new bound states, the energies of which are deduced from

$$1-t_1t_2g_{12}g_{21} = 0 \Rightarrow \nu_b = \frac{A\pm\sqrt{A^2-4B}}{B}, \tag{19}$$

where $A = h_1g_{11}+h_2g_{22}$, $B = h_1h_2(g_{11}g_{22}-g_{12}g_{21})$, and $h_i = h_0(\boldsymbol{x}_i)$. The new bound state solutions have the following properties: i) ν_b cannot reach zero just as for the single impurity case; ii) the new ν_b's are different from $\nu_{b,1}$ or $\nu_{b,2}$; iii) the new ν_b's are also positive-definite, meaning that they also descend down from the UHB; iv) most importantly, they become smaller, i.e. closer to the Fermi energy. In the single impurity case, the value of h_0 is bounded as $|\delta\langle n_f\rangle| \leq$

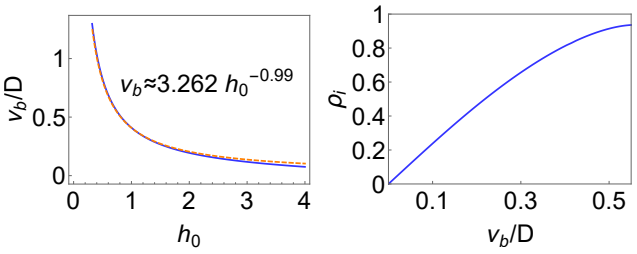


FIG. 3. The bound state energies ν_b plotted as a function of the effective rotor impurity potential h_0 (3a) and the spectral weights ρ_i at given energy ν_b (3b).

1 which further puts bounds on ν_b from below. However, in Eq. (19), when the two impurity potentials are close enough, we have $B \ll A$. By expanding Eq. (19) in terms of small B, we find

$$\nu_b \sim 1/A = 1/(h_1 g_{11} + h_2 g_{22}). \tag{20}$$

Let $h_1 = h_2 = h_0$, and $g_{11} = g_{22} = g_{00}$, and compare Eq. (20) with the single impurity case, $\nu_{b,\text{single}} \simeq g_{00} h_0$. Therefore, the new bound state can be considered as generated by an effective and larger $h_0' \simeq 2h_0$. In other words, the strength of impurities close together effectively adds up to produce bound states with lower and lower energies. Similar approximation can be made by considering the T-matrix of M impurities (see Supplement Materials), i.e. when these impurities are sufficiently close, the bound state of the lowest energy can be viewed as generated by a single impurity with all the impurity strength superimposed $h_0' \simeq \sum_{m=1,\ldots,M} h_m g_{mm}$, which The bound state energies $\nu_b \sim 1/h_0'$ is pushed closer to the Fermi energy as the number of impurities in a cluster increases.

Therefore, it is reasonable to use h_0, which now can go beyond the upper bound in the single impurity case, as a tuning parameter for impurity concentration. We shall compute the bound state energies and their corresponding spectral weights as a function of arbitrary h_0, and use the results to qualitatively explain experimental observation for doped samples. We plot the energies of the in-gap states ν_b as a function of the impurity potential strength h_0 in Fig. (3a) and the corresponding spectral weights in Fig. (3b). Note that the asymptotic behavior is $\nu_b \sim 1/h_0$, which forbids the impurity state from reaching zero, i.e. the Fermi energy of the bulk. The corresponding spectral weight $\rho_i = \frac{(\Lambda_0(\nu_b)^2 - \pi^2 \rho_0(\nu_b)^2)}{|h_0(\nu_b\ \partial_\nu \Lambda_0(\nu_b) + \Lambda_0(\nu_b))|}$ decreases when ν_b approaches zero.

Experimental implications. From those results, we can explain the difference between the LDOS on the Cl^- site and the Ca^{2+} site. The LDOS of Cl^- vacancy is well explained by the single impurity solution, while that of a single Ca^{2+} vacancy is much closer to the Fermi energy. To explain the discrepancy, we note that the impurity potential of a Ca^{2+} vacancy acts simultaneously on its *four* neighboring Cu sites (see Supplement Materials), forming a four-impurity cluster. Thus, according to our approximation for the multi-impurity case, the peak position (relative to the Fermi energy) of Ca^{2+} vacancy should be about $1/4$ of that for the Cl^- site. The experimental results in Ref. [4] give $\omega_b(Cl^-) \simeq 1.8eV$ and $\omega_b(Ca^{2+}) \simeq 0.5eV$, showing a quantitative agreement with our theory. A recent STM measurement[20] further confirmed our quantitative prediction with explicit comparison of measurements on single-impurity and two-impurity clusters.

Discussion. Our work suggests that the observed V-shaped LDOS suppression is a generic feature of Mott insulators with or without magnetism. This is manifested by the special form of the effective rotor impurity potential, $\hat{H}_{X,\boldsymbol{x}_0} = ih_0(X^*_{\boldsymbol{x}_0}\partial_t X_{\boldsymbol{x}_0} - h.c.)$ which vanishes for $\nu = 0$ as long as the system is still in the Mott insulator phase. More generally, the vanishing of LDOS reflects an exact zero of the local Green's function of the *parent Mott phase* rather than just the zeros of the spectral function, as we show in the Supplement Materials. This exact zero of the local Green's function is a consequence of the Luttinger surface of the electrons' Green's function in $\boldsymbol{k}$-space at the Fermi energy. We propose that this Luttinger surface has topological stability related to the Mott gap, in a sense similar to the stability of a Fermi surface[21, 22]. Exactly how such protection works is an intriguing open question for future studies.

The alignment of our theory with the experimental observations is also a demonstration of the emergence principle in the strongly correlated systems. Conventionally, the approach to such impurity problem would be implementing the T-matrix method directly with the physical Green's functions, such as in the simulation of Ref. [14]. But such efforts have failed to explain the key aspects of the experimental observations. In our approach, the Luttinger point physics is captured through the proper treatment of the constraint to obtain the effective rotor impurity potential, Eq. (11).

While being able to account for many aspects of the impurity effects, our ultimate goal is to understand how finite concentration of impurities or holes eventually causes the Mott phase, and the concomitant Luttinger surface, to collapse, which further leads to all these fascinating phenomena in the underdoped regime. The slave rotor theory has the advantage of accounting for the Luttinger points or surfaces. Other related methods, even though may be capable of describing the finite doping phases, are not found to describe such impurity states. The current work suggests that future development of the formalism places a minimal requirement, viz. to capture the Luttinger surfaces of the half-filling limit.

Summary. We have studied the local density of states of a single impurity in the Mott insulator. Using a slave rotor method, we solve the rotor impurity problem using the T-matrix method, and find that the solution accounts for both of the key features of the observed local density of states on a single impurity regarding i) positions and amplitudes of the in-gap spectral weights; ii) the spectral weight transfer from the UHB to the LHB. Further analysis of the solutions for multiple impurities shows that high impurity concentration can be accounted for by a larger effective impurity potential for the rotor fields. We have emphasized that the Luttinger surfaces

play an important role in our results.

We would like to acknowledge useful discussions with Y. Y. Wang. This work has primarily been supported by the NSF under Grant No. DMR-2220603, and by the Robert A. Welch Foundation Grant No. C-1411 and the Vannevar Bush Faculty Fellowship ONR-VB N00014-23-1-2870. W.D. was supported by the National Key R&D Program of the MOST of China under Grant No. 2022YFA1602603 and the Startup Grant No. S020118002/002 of Anhui University.

* wenxinding@gmail.com

[1] P. A. Lee and X. Wen, Rev. Mod. Phys. **78**, 17 (2006).
[2] J. Zaanen, G. a. Sawatzky, and J. W. Allen, Phys. Rev. Lett. **55**, 418 (1985).
[3] P. W. Anderson, Phys. Rev. **79**, 350 (1950).
[4] C. Ye, P. Cai, R. Yu, X. Zhou, W. Ruan, Q. Liu, C. Jin, and Y. Wang, Nat. Commun. **4**, 1365 (2013).
[5] P. Cai, W. Ruan, Y. Peng, C. Ye, X. Li, Z. Hao, X. Zhou, D.-H. Lee, and Y. Wang, Nat. Phys. **12**, 1047 (2016).
[6] B. Keimer, S. a. Kivelson, M. R. Norman, S. Uchida, and J. Zaanen, Nature **518**, 179 (2015).
[7] Z. Liu and E. Manousakis, Phys. Rev. B **45**, 2425 (1992).
[8] D. Poilblanc, D. J. Scalapino, and W. Hanke, Phys. Rev. Lett. **72**, 884 (1994).
[9] W.H. Leong, S.l. Yu, T. Xiang, and J.X. Li, Phys. Rev. B **90**, 245102 (2014).
[10] I. Dzyaloshinskii, Phys. Rev. B **68**, 85113 (2003).
[11] R. M. Konik, T. M. Rice, and A. M. Tsvelik, Phys. Rev. Lett. **96**, 086407 (2006).
[12] K.-Y. Yang, T. M. Rice, and F.-C. Zhang, Phys. Rev. B 73, 174501 (2006).
[13] K. B. Dave, P. W. Phillips, and Charles L. Kane, Phys. Rev. Lett. **110**, 090403 (2013).
[14] Z. Sun, J. M. Guevara, S. Sykora, E. M. Pärschke, J. van den Brink, K. Manna, A. Maljuk, S. Wurmehl, B. Büchner, and C. Hess, Phys. Rev. Research, **3**, 023075 (2021).
[15] Wenxin Ding, Rong Yu, Qimiao Si and Elihu Abrahams, Phys. Rev. B, **100**, 235113 (2019).
[16] S. Florens and A. Georges, Phys. Rev. B **66**, 165111 (2002).
[17] S. Florens and A. Georges, Phys. Rev. B **70**, 035114 (2004).
[18] S.-S. Lee and P. A. Lee, Phys. Rev. Lett. **95**, 036403 (2005).
[19] E. N. Economou, *Green's Functions in Quantum Physics*, Springer Series in Solid-State Sciences, Vol. 7 (Springer Berlin Heidelberg, Berlin, Heidelberg, 2006).
[20] H. Li, S. Ye, J. Zhao, C. Jin, and Y.Y. Wang, Sci. Bull., **66**, 1395 (2021).
[21] G. E. Volovik, The Universe in a Helium Droplet (Oxford University Press, 2009).
[22] P. Hořava, Phys. Rev. Lett. **95**, 16405 (2005).